Publication details:	Jain R, Zhao K, Sheridan JM, Heinlein M, Kupresanin F, Abeysekera W, Hall C, Rickard J, Bouillet P, Walczak H, Strasser A, Silke J, Gray DHD. Dual roles for LUBAC signaling in thymic epithelial cell development and survival. *Cell Death and Differentiation.* 2021 28(10):2946-2956
Final authenticated version Is available online at:	https://doi.org/10.1038/s41418-021-00850-8

Dual roles for LUBAC signaling in thymic epithelial cell development and survival

Reema Jain[1,2,#], Kelin Zhao[1,2], Julie M. Sheridan[1,2], Melanie Heinlein[1,2*], Fiona Kupresanin[1^], Waruni Abeysekera[1], Cathrine Hall[1,2], James Rickard[1,2], Philippe Bouillet[1,2], Henning Walczak[3,4], Andreas Strasser[1,2], John Silke[1,2], Daniel H.D. Gray[1,2$]

[1]Walter and Eliza Hall Institute of Medical Research, Melbourne, VIC, Australia; [2]Department of Medical Biology, University of Melbourne, Melbourne, VIC, Australia; [3] Centre for Cell Death, Cancer and Inflammation, UCL Cancer Institute, University College London, London, UK, [4] Centre for Biochemistry, University of Cologne, Cologne, Germany

[#] Current address Fred Hutchinson Cancer Research Center, Seattle, Washington, USA.

* Current address Genentech, South San Francisco, USA

^ Current address ANZAC Research Institute, Concord, Australia

[$]Correspondence to: dgray@wehi.edu.au

T: +61 3 9345 2741

F: +61 3 9347 0852

Short Title: Essential functions for LUBAC in thymic epithelium

Abstract

Thymic epithelial cells (TECs) form a unique microenvironment that orchestrates T cell differentiation and immunological tolerance. Despite the importance of TECs for adaptive immunity, there is an incomplete understanding of the signalling networks that support their differentiation and survival. We report that the linear ubiquitin chain assembly complex (LUBAC) is essential for medullary TEC (mTEC) differentiation, cortical TEC survival and prevention of premature thymic atrophy. TEC-specific loss of LUBAC proteins, HOIL-1 or HOIP, severely impaired expansion of the thymic medulla and AIRE-expressing cells. Furthermore, HOIL-1-deficiency caused early thymic atrophy due to Caspase-8/MLKL-dependent apoptosis/necroptosis of cortical TECs. By contrast, deficiency in the LUBAC component, SHARPIN, caused relatively mild defects only in mTECs. These distinct roles for LUBAC components in TECs correlate with their function in linear ubiquitination, NFκB activation and cell survival. Thus, our findings reveal dual roles for this critical cell signaling hub in TEC differentiation and survival.

Introduction

The differentiation of haematopoietic progenitors into naive T cells in the thymus is governed by thymic epithelial cells (TECs). Specialized TEC subtypes direct distinct quality control processes in thymocyte differentiation. Cortical thymic epithelial cells (cTECs) mediate early events, including T cell lineage commitment, proliferation and positive selection of cells expressing TCRs capable of interacting with self-peptide/MHC complexes (1). By contrast, medullary thymic epithelial cells (mTECs) are important for thymic negative selection and the generation of $FOXP3^{+}$ regulatory T (Treg) cells, thus limiting the risk of autoimmunity (2). Medullary TECs are uniquely adapted for the induction of immunological tolerance because they express thousands of tissue-specific antigens that greatly increase the scope of thymic negative selection. This property is mediated in mTEC subtypes by the transcriptional regulators AIRE and FEZF2 (2, 3). These essential functions of TEC in immunity and tolerance have generated considerable interest in the molecular mechanisms of their differentiation and maintenance.

Members of the tumour necrosis factor (TNF) and TNF receptor (TNFR) superfamilies (i.e. the TNFSF and TNFRSF) and NF-κB transcription factors are critical for TEC differentiation and the establishment of thymic tolerance (4). Signalling through RANK is required for mTECs during development, whereas signals from other TNFRSF members co-ordinate the maintenance of postnatal mTECs (5, 6). Ligation of the TNFRSF members CD40, RANK and lymphotoxin beta receptor (LTβR) is required for the development of the key tolerogenic mTEC populations, such as $AIRE^{pos}$ and $FEZF2^{pos}$ cells (3, 5, 7-9). Yet, precisely how these signals are integrated to direct TEC fate, function and survival remains poorly understood.

LUBAC is a component of TNFR1 and CD40 receptor signalling complexes (10, 11) that attaches linear ubiquitin chains to signal transducers and/or regulators of the canonical NF-κB pathway, including RIPK1, TRADD, NEMO and TNFR1 itself (10, 12, 13). LUBAC is a ~600-kD ubiquitin E3 complex composed of three proteins: SHANK-associated RH domain interacting protein (SIPL1/SHARPIN), C3HC4-type zinc finger containing 1 (RBCK1/HOIL-1) and the catalytic component, ring finger protein 31 (RNF31/HOIP) (10, 12, 14-16). Mutations of these LUBAC components perturb innate and adaptive immune responses (10, 17, 18). Patients with loss-of-function mutations in HOIL-1 or HOIP were found to be T cell deficient and (in one patient) had greatly reduced T-cell receptor excision circles, indicating impaired thymic function (17, 18).

There is a differential requirement for HOIP, HOIL-1 and SHARPIN for LUBAC function, signal transduction, differentiation and cell death. Deficiency in HOIP or HOIL-1 completely abolishes LUBAC activity, impairs NF-κB activation and promotes cell death (10, 15, 19-21). By contrast, SHARPIN-deficient cells can carry out diminished linear ubiquitination via HOIL-1/HOIP complexes, attenuated activation of NF-κB and JNK signaling pathways and are also sensitized to cell death (10, 21-23). Importantly, LUBAC functions in NF-κB activation and cell survival can be independent (24).

The *in vivo* consequences of these defects vary according to cell type and developmental context. Complete HOIP- or HOIL-1-deficiency causes embryonic lethality due to TNF-induced vascular defects (21, 25). The loss-of-function SHARPIN mutant mice, *cpdm*, are viable but succumb to severe dermatitis from approximately 6 weeks of age (26, 27), primarily due to sensitization to TNF-induced cell death via apoptosis or necroptosis (10, 21-23). Roles for LUBAC in lymphocyte

differentiation, activation and survival (e.g. (20, 28, 29)) have also been reported. Key questions in the field remain how complete or partial loss of LUBAC function impacts various tissues and how these defects influence inflammatory and immune pathology (17, 18).

Given the importance of TNFRSF signaling in TEC and thymic tolerance (7, 9, 30, 31), we investigated whether LUBAC function was required for TEC development and homeostasis. Conditional ablation of HOIP or HOIL-1 in TEC caused severe thymic atrophy and T cell deficiency. HOIL-1 was required for the development of the thymic medulla in young mice and the maintenance of cTEC in adults. Thymic atrophy and the demise of HOIL-1-deficient TECs was driven in part by caspase-8/MLKL-driven apoptosis/necroptosis; blockade of this process restored cortical and medullary microenvironments and thymic T cell production. Conversely, only mild disruption of the thymic microenvironment was observed in SHARPIN-deficient mice, confined to a defect in immature mTECs that was not related to cell death. These findings identify LUBAC as an essential signaling hub with distinct roles in mTEC development, cTEC survival and thymic function.

Results

LUBAC proteins HOIL-1 and HOIP in TECs are essential to maintain thymic function

We first assessed expression of the three LUBAC components in RNAseq data from TEC subpopulations purified from young adult 8 week-old mice. TEC can be sub-divided into three main populations: cTEC, MHC II^{low} mTEC (termed mTEC^{low}) that contain a mixture of precursors and differentiated cells, and MHC II^{high} mTEC (termed mTEC^{high}) including cycling cells and the AIRE+ subset(30). All three known LUBAC components were transcribed in all TEC subsets,

with *Rnf31* (encoding HOIP) relatively lower in mTEC^{high}, while mTEC^{low} expressed the highest levels of *Sipl1* (encoding SHARPIN) (**Figure 1A**). To determine the roles of LUBAC components in TECs *in vivo,* we generated mice with *Foxn1*^{Cre}-driven deletion of *Rbck1* or *Rnf31*, hereafter termed *Hoil-1*$^{\Delta Foxn1}$ and *Hoip*$^{\Delta Foxn1}$, respectively (20, 21, 25) (specific deletion confirmed in **Figure S1A**). Mice in both of these strains were viable, reproduced normally and had no overt health problems. The role of SHARPIN in TEC development was assessed in the spontaneous loss-of-function mutant *cpdm* mouse strain (*Sh*$^{cpdm/cpdm}$) (26, 27), prior to the onset of inflammation. We observed a modest reduction in the thymic cellularity of *Sh*$^{cpdm/cpdm}$ mice; however, TEC-specific loss of HOIL-1 or HOIP caused severe thymic atrophy in adult mice (**Figure 1B**).

We tracked thymocyte differentiation *Hoil-1*$^{\Delta Foxn1}$ mice by analyzing CD4 vs. CD8 expression and observed loss in all major stages of T cell differentiation (**Figure 1C, Figure S1B**). Deeper analysis of CD4$^-$CD8$^-$ double negative (DN) precursor stages revealed a proportional block at the DN3 stage of differentiation and numerical loss in all thymocyte precursor stages in *Hoil-1*$^{\Delta Foxn1}$ mice (**Figure S1C**). Thymic Treg cell production in 8-week-old *Hoil-1*$^{\Delta Foxn1}$ mice was virtually extinguished in the severely atrophic thymi (**Figure S1D**). These data show that TEC-specific HOIL-1 deletion led to severe thymic hypotrophy and markedly impaired T cell differentiation.

We then compared the thymic phenotype of young **(Figure 1D)** and young adult *Hoip*$^{\Delta Foxn1}$ mice **(Figure S1E-G)** and found that they closely resembled that of *Hoil-1*$^{\Delta Foxn1}$ mice, with severe deficiency in all major thymocyte subsets. Thus, HOIP and HOIL-1 are critical in TECs for establishing or maintaining thymic function, consistent with the essential roles of these proteins in LUBAC activity (21).

The thymic defects in adult *Hoil-1*$^{\Delta Foxn1}$ mice caused T cell lymphopenia in peripheral lymphoid tissues (**Figure S2A**). Both CD4^{+} and CD8^{+} T cells were diminished and, consistent with the thymic atrophy, naïve CD44^{low} CD62L^{high} populations were particularly affected with homeostatic expansion of CD122^{+} "virtual" memory cells (**Figure 1E, F, Figure S2B, C**). Although the proportions of proliferating Ki67^{+} T cells and FOXP3^{+} Treg cells were increased in 8-week-old *Hoil-1*$^{\Delta Foxn1}$ mice, the overall numbers were largely normal (**Figure S2D, E**). This loss of naïve T cell populations yet maintenance of the virtual memory and regulatory subsets is consistent with the greater reliance on thymic output of the former (32). These defects extended to the TCR repertoire, with alterations in T cells expressing distinct TCRβ chains (**Figure S2F**).

We then assayed thymus size throughout ontogeny to determine whether HOIL-1 was required in TECs for thymic development or homeostasis. Overall thymic cellularity immediately following birth was normal in *Hoil-1*$^{\Delta Foxn1}$ mice but by day 3-4 mild thymic hypotrophy was evident (**Figure 1G**). All major thymocyte subsets, including Treg cells, were diminished and DN1 and DN3 precursor populations were reduced in 4-day-old *Hoil-1*$^{\Delta Foxn1}$ mice (**Figure S3A-C**). T cell lymphopenia was not yet evident in the spleen, although a mild reduction in the proportion of naïve CD4+ T cells was detected in 4-day-old *Hoil-1*$^{\Delta Foxn1}$ mice (**Figure S3D-F**). Thymus size in *Hoil-1*$^{\Delta Foxn1}$ mice peaked at days 9-10 but then atrophied, with approximately 12-fold lower thymic cellularity at 8 weeks of age compared to controls (**Figure 1G**). These data reveal a differential requirement for LUBAC components in TEC maintenance, with HOIL-1 and HOIP essential for thymic function beyond the perinatal stage and the establishment of a normal naïve T cell pool.

TECs require HOIL-1 or HOIP for their homeostasis

We next investigated the role of HOIL-1 or HOIP in TEC homeostasis at key time points. Low numbers of TECs could be recovered from the atrophied thymi of aged-matched 13-week-old *Hoil-1$^{\Delta Foxn1}$* (**Figure 2A**) and *Hoip$^{\Delta Foxn1}$* mice (**Figure 2B**). We analysed the phenotype of those TECs that could be recovered and found very similar profiles in both *Hoil-1$^{\Delta Foxn1}$* or *Hoip$^{\Delta Foxn1}$* mice, with severe loss in the number of mTEC (Ly51^{-}UEA-1^{+}) **(Figure 2C-F)**. Examination of the thymic architecture of 8-week-old *Hoil-1$^{\Delta Foxn1}$* or *Hoip$^{\Delta Foxn1}$* mice revealed extensive disruption of cortical and medullary regions (labelled with anti-keratin-8 versus anti-keratin-5/UEA-1), including the AIRE^{+} compartment, which had almost disappeared **(Figure 2G-L)**. The loss of TEC in adult *Hoil-1$^{\Delta Foxn1}$* and *Hoip$^{\Delta Foxn1}$* mice was characterized by large epithelial cell-free areas and prominent ERTR7^{+} fibroblastic remodeling (**Figure 2G-L**). These data indicate that HOIL-1 and HOIP are required for the differentiation and/or homeostasis of all major TEC subpopulations in the adult thymus. The identical impact of TEC-specific HOIL-1- or HOIP-deficiency on the thymus and TEC phenotype is consistent with observations in other tissues and the complete ablation of LUBAC-mediated linear ubiquitination caused by loss of either protein (10, 15, 21).

We next sought to distinguish whether LUBAC activity was required for TEC differentiation or homeostasis. We assayed TEC composition during the development of *Hoil-1$^{\Delta Foxn1}$* mice and observed a slight reduction in total TEC numbers as early as E15.5 that worsened in 4-day postnatal mice **(Figure 3A)**. Flow cytometric analysis was used to quantify the major subpopulations of EpCAM^{+} TECs: cTEC and mTEC, and the mTEC subpopulations mTEC^{high} (Ly51^{-}UEA-1^{+}MHCII^{+}CD80^{high}) and mTEC^{low} (Ly51^{-}UEA-1^{+}MHCII^{+}CD80$^{low/-}$) cells that become apparent in day 4 mice **(Figure 3B-D)**. We found a severe deficit in mTEC in embryonic and neonatal thymi

from *Hoil-1*$^{\Delta Foxn1}$ mice (**Figure 3B-D**), including the tolerogenic AIRE^{+} population (**Figure 3E**). The proportion of Ki67^{+} TECs was increased in E15.5 and day 4 *Hoil-1*$^{\Delta Foxn1}$ mice, suggesting specific loss of non-proliferating TECs and/or compensatory proliferation of remaining cells (**Figure 3F, G**). Therefore, although TECs from *Hoil-1*$^{\Delta Foxn1}$ mice were capable of proliferation and differentiation into the major TEC subpopulations, they were unable to maintain normal numbers. By contrast, relatively normal numbers of cTECs were recovered at these stages (**Figure 3C, D**).

The thymic architecture of neonatal *Hoil-1*$^{\Delta Foxn1}$ mice was also perturbed. Although the distribution of ERTR7^{+} fibroblasts was comparable, medullary regions (labelled with anti-keratin-5, UEA-1 and AIRE) were fewer and smaller in *Hoil-1*$^{\Delta Foxn1}$ mice at day 4 **(Figure 3H-J**). Consistent with the flow cytometric analysis, a normal network of K8^{+} cTECs was apparent in thymi from neonatal *Hoil-1*$^{\Delta Foxn1}$ mice (**Figure 3H**). We conclude that HOIL-1 is not required for mTEC differentiation *per se* but is essential for the expansion and maintenance of all mTEC subpopulations in the perinatal thymus. Furthermore, HOIL-1-mediated signals are not required for the early differentiation and expansion of cTECs yet is required for their maintenance and thymic function later in life (**Figure 1, 2**).

HOIL-1 is required to prevent TEC necroptosis to sustain thymic function

To explore how the loss of LUBAC function leads to these outcomes, we performed RNAseq analysis on FACS-purified cTEC and mTEC^{high} from 2-week-old *Hoil-1*$^{lox/lox}$ (control) and *Hoil-1*$^{\Delta Foxn1}$ mice. We selected this age because: 1) it immediately precedes severe thymic atrophy, therefore the relevant transcriptional changes should be underway, 2) sufficient numbers of TEC

198 could be recovered and 3) the relative expression profiles of the LUBAC components was
199 equivalent to young adult mice (**Figure S4A**). Visualization of the relationships among the
200 populations in a multi-dimensional scaling plot showed: (1) that the 3 biological replicates
201 clustered together closely, indicating low experimental variability, (2) the first dimension
202 distinguished cTEC from mTEC^{hi}, and (3) the second dimension distinguished the transcriptional
203 impact of *Hoil-1*-deficiency (**Figure 4A**). Large transcriptional changes were caused by HOIL loss
204 in cTEC and mTEC^{high}, with ~3,000 and ~5,700 genes reaching the thresholds for statistical
205 significance, although these generally had modest overall expression levels (log expression) or
206 fold-changes (**Figure 4B**). KEGG pathway analyses of differentially expressed genes revealed
207 enrichment in those associated with cell adhesion, ECM interaction and various signaling
208 pathways in cTECs, including several metabolic pathways and cell cycle regulators in mTEC^{hi}
209 **(Figure S4B, C)**. Interestingly, we observed enrichment of genes involved in regulation of cell
210 projection organization and morphology among HOIL-1 induced transcripts in cTEC (**Figure S4**
211 **D-F**); processes recently implicated in thymic regeneration from aged-related involution (33).
212
213 LUBAC-dependent cell signaling can be required to prevent aberrant cell death via caspase-8-
214 dependent apoptosis and/or by MLKL-dependent necroptosis, depending on the cell type (20-22,
215 24, 29, 34). Hierarchical clustering of the transcriptional profiles of genes involved in receptor-
216 mediated programmed cell death was visualized using heatmaps (**Figure 4C**). These clearly
217 distinguished TEC subsets from the two genotypes, indicating that substantial differences in this
218 pathway were induced by the loss of HOIL-1 (**Figure 4C**). Among these changes, the upregulation
219 of *Mlkl* and *Casp8* was a distinguishing feature of cTECs and mTEC^{high} cells isolated from 2-
220 week-old *Hoil-1*$^{\Delta Foxn1}$ mice. These findings suggest that the loss of HOIL-1 in TECs had sensitized

them to MLKL-dependent necroptosis and/or caspase-8-driven apoptosis just prior to the onset of severe thymic atrophy.

To test whether the TEC defects observed in HOIL-1-deficient mice were caused by the induction of cell death, we generated *Hoil-1$^{\Delta Foxn1}$Casp8$^{-/-}$Mlkl$^{-/-}$* mice in which both apoptotic and necroptotic pathways are non-functional (35). We first established that young *Casp8$^{-/-}$Mlkl$^{-/-}$* mice had normal TN, DP and SP thymocyte differentiation and splenic T cell homeostasis (**Figure 4D, E, S5**), extending on previous analyses (20, 35) and isolating any phenotypes observed in the compound mutants to changes in the TEC compartment. In striking contrast to the severe thymic atrophy and T cell lymphopenia observed in *Hoil-1$^{\Delta Foxn1}$* mice, *Hoil-1$^{\Delta Foxn1}$Casp8$^{-/-}$Mlkl$^{-/-}$* mice had normal thymic cellularity and near complete restoration of the peripheral T cell population (**Figure 4D, E**). This finding indicates that the combined loss of Caspase-8 and MLKL prevented the thymic atrophy observed in adult *Hoil-1$^{\Delta Foxn1}$* mice.

Interestingly, the rescue of thymic function was driven by only partial restoration of the thymic microenvironment. *Hoil-1$^{lox/lox}$Casp8$^{-/-}$Mlkl$^{-/-}$* control mice had a reduction in overall TEC number compared to *Hoil-1$^{lox/lox}$* control mice due to loss of mTEC (**Figure 4F, G**). TEC number was further decreased in *Hoil-1$^{\Delta Foxn1}$Casp8$^{-/-}$Mlkl$^{-/-}$* mice, yet was higher than the atrophied thymus of *Hoil-1$^{\Delta Foxn1}$* mice, suggesting only a portion of TEC were rescued (**Figure 4F**). This rescue was accounted for mainly by increased mTEC, although there was a trend (not statistically significant) towards higher cTEC in *Hoil-1$^{\Delta Foxn1}$Casp8$^{-/-}$Mlkl$^{-/-}$* compared to *Hoil-1$^{\Delta Foxn1}$* mice (**Figure 4G, H**). Immunofluorescent staining of thymic sections from 8-week-old *Hoil-1$^{\Delta Foxn1}$Casp8$^{-/-}$Mlkl$^{-/-}$* mice confirmed that the rescue of HOIL-1-deficient TEC was partial, demonstrating small, isolated

medullary islets composing a reduced area compared to the large, confluent medulla of thymi from control mice (**Figure 4I, J, S5F**). In contrast, a normal, confluent $K8^+$ cTEC network and cortical microenvironment was observed (**Figure 4I, J**), contrasting the near complete loss of these cells and regions in *Hoil-1*$^{\Delta Foxn1}$ mice (**Figure 2 E, F**). Therefore, caspase-8 and MLKL deficiency restored the cortical microenvironment and thymic lymphopoiesis in *Hoil-1*$^{\Delta Foxn1}$ mice, but only partially restored the thymic medulla.

Collectively, these findings demonstrate that a broad transcriptional program is coordinated in TEC by HOIL-1-mediated signals and that antagonism of TEC necroptosis/apoptosis within this program is a critical mechanism supporting thymic function.

SHARPIN is required for normal mTEC^{low} compartment

The severe thymic atrophy observed in *Hoil-1*$^{\Delta Foxn1}$ and *Hoip*$^{\Delta Foxn1}$ mice prompted us to also explore the function of the third LUBAC component, SHARPIN, in TECs and thymic function. To circumvent potentially confounding effects of the psoriasis-like inflammatory syndrome in these *Sh*$^{cpdm/cpdm}$ mice (26), we analyzed TECs and thymic function in *Sh*$^{cpdm/cpdm}$ mice prior to the development of dermatitis. Consistent with previous data (20), we recovered normal proportions of DP thymocytes in *Sh*$^{cpdm/cpdm}$ mice, indicating that no stress-related atrophy had occurred. Nevertheless, mild thymic hypotrophy was accompanied by a trend towards lower TEC numbers (**Figures 1B and 5A**), with half the normal number of $mTEC^{low}$ in *Sh*$^{cpdm/cpdm}$ mice (**Figure 5B, C**). The numbers of cTEC, $mTEC^{high}$, $AIRE^+$ TECs and the proportions of proliferating $Ki67^+$ TECs were similar in controls and *Sh*$^{cpdm/cpdm}$ mice (**Figure 5C, S6A, S6B**). The observed $mTEC^{low}$ defect was not recapitulated in *Sh*$^{cpdm/cpdm}$→ wt (Ly5.1) hematopoietic chimeras (**Figure S6C-F**),

indicating that the mTEC^{low} defect was a primary consequence of the loss of SHARPIN in the thymic stroma. Analysis of the thymic architecture of *Sharpin*$^{cpdm/cpdm}$ mice revealed mild disruption of the thymic medulla compared to controls, although the location and frequency of AIRE^{+} TECs and ERTR7^{+} fibroblasts were comparable to controls (**Figure 5D-F)**. We conclude that SHARPIN-mediated signals are required specifically to maintain the mTEC^{low} population.

SHARPIN is required to antagonize TNF-induced cell death in certain contexts (10). This pro-survival activity is not dependent on NF-κB signaling but involves direct linear ubiquitination of the TNFR1 signalling complex, recruitment of IKK complexes to phosphorylate RIPK1 and prevent caspase-8-mediated apoptosis or RIPK3/MLKL-dependent necroptosis (10, 22-24). To test whether the loss of mTEC^{low} in *Sh*$^{cpdm/cpdm}$ mice was driven by TNF-induced, caspase-8-dependent apoptosis or RIPK3- and MLKL-dependent necroptosis, we assayed for rescue of the phenotype when these pathways were disabled. Genetic ablation of both caspase-8-driven apoptosis and RIPK3/MLKL-dependent necroptosis in *Sh*$^{cpdm/cpdm}$*Casp8*$^{+/-}$*Ripk3*$^{-/-}$ and *Sh*$^{cpdm/cpdm}$*Casp8*$^{-/-}$*Mlkl*$^{-/-}$ mice failed to rescue the loss of mTEC^{low} observed in *Sh*$^{cpdm/cpdm}$ mice **(Figure 5G**). Consistent with this finding, *Sh*$^{cpdm/cpdm}$*Tnf*$^{-/-}$ mice also exhibited the loss of mTEC^{low} (**Figure 5H**). These data indicate that cell death driven by TNF or other death ligands was not the cause of the mTEC defect in *Sh*$^{cpdm/cpdm}$ mice. Therefore, we conclude that LUBAC deprived of SHARPIN sustains sufficient activity to support TEC survival and thymic function but cannot maintain a normal mTEC^{low} population.

Discussion

The attachment of Met1-linked "linear" chains of ubiquitin to proteins has emerged as a key regulator of NF-κB and cell death signaling in inflammation, cell survival and differentiation (36). LUBAC is the only E3 ligase complex known to mediate this form of ubiquitination and it is composed of SHARPIN, HOIL-1 and HOIP. The loss of HOIP or HOIL-1 completely abolishes linear ubiquitination. SHARPIN deficiency only partially reduces this activity, with residual HOIL-1/HOIP complexes sufficient to sustain some LUBAC function in NF-κB-related programs and the prevention of cell death induced by death ligands other than TNF (10, 12, 14, 21, 22, 25, 34). Given the critical roles of TNFR family members and NF-κB signaling in mTEC differentiation and homeostasis (4), we tested the importance of LUBAC function in TECs. Our data highlight essential roles for LUBAC signalling in mTEC development on one hand, and cTEC survival in adulthood on the other.

Conditional ablation of either HOIL-1 or HOIP in TECs greatly diminished all mTEC subsets and the formation of the medulla early in life. This phenotype resembles that observed in mice with compound deficiency in the TNFRSF members RANK plus CD40 or LTβR plus CD40 (7, 9, 37), or those with loss of the NF-κB signaling proteins NIK, TRAF6 or REL-B, where severe loss of multiple mTEC subpopulations was observed (4). It is likely that the requirement for the LUBAC for optimal NF-κB signaling explains the mTEC defects observed in HOIL-1-deficient mice. However, we also found that *Hoil-1*$^{\Delta Foxn1}$ mice succumbed to premature thymic atrophy associated with loss of cTEC in adult animals, which appears to be a novel phenotype. These cTEC defects are highly likely to cause the collapse of thymic function, since most thymocyte proliferation is driven by this microenvironment. It is possible that LUBAC signals may be required for an aspect

of cTEC function critical to the production of DP thymocytes, the loss of which then feeds back to cause more severe defects in this compartment. Although Shen *et al.* reported loss of cTEC in young *Nik*$^{\Delta Foxn1}$ mice, this phenotype was likely a secondary consequence of the severe autoimmune hepatitis and pneumonitis in these mice, resulting in the stress-induced loss of DP thymocytes (38) required to support this thymic microenvironment. By contrast, *Hoil-1*$^{\Delta Foxn1}$ and *Hoip*$^{\Delta Foxn1}$ mice were overtly healthy and had no signs of stress-induced DP thymocyte death.

The spontaneous upregulation of genes involved in apoptosis and necroptosis in HOIL-1-deficient TEC hinted that the induction of aberrant cell death might drive their loss; a notion supported by the rescue of the thymic cortex and thymic function in *Hoil-1*$^{\Delta Foxn1}$*Casp8*$^{-/-}$*Mlkl*$^{-/-}$ mice. This finding is in accord with observations that LUBAC-deficiency in certain cell types can predispose them to TNF-induced apoptosis (which is caspase-8-dependent) or necroptosis (which is RIPK1/RIPK3/MLKL-dependent)(10, 21, 22, 25, 39). Although our genetic data implicate aberrant cell death in the TEC loss, cortical collapse and thymic atrophy observed in *Hoil-1*$^{\Delta Foxn1}$ mice, only a modest increase in overall TEC number was observed in *Hoil-1*$^{\Delta Foxn1}$*Casp8*$^{-/-}$*Mlkl*$^{-/-}$ mice, despite restoration of a normal, confluent K8^{+} cTEC network. This observation may reflect a technical limitation of flow cytometric analysis of TEC, whereby the recovery of cTEC greatly underestimates the total number of these cells, as established by Sakata, *et al.* (40). Other approaches will be required to confirm whether loss of LUBAC function primarily impacts cTEC survival *in vivo*. Alternatively (or in addition), defective regulation of cTEC morphology may influence the atrophy observed in *Hoil-1*$^{\Delta Foxn1}$ mice. We found changes in the expression of genes regulating cellular projections in cTEC from *Hoil-1*$^{\Delta Foxn1}$ mice, reminiscent of features reported in thymic regeneration in aged mice that were independent of cTEC numerical changes(33). While

the precise mechanisms remain to be determined, it is clear that the main lymphopoietic cTEC niches were restored in *Hoil-1*$^{\Delta Foxn1}$*Casp8*$^{-/-}$*Mlkl*$^{-/-}$ mice, uncovering a critical signaling axis in the cTEC essential for thymic function.

We also found that the restoration of the medulla was not complete in *Hoil-1*$^{\Delta Foxn1}$*Casp8*$^{-/-}$*Mlkl*$^{-/-}$ mice, therefore it is likely LUBAC modulates other signals supporting TEC expansion and/or survival. In this regard, we note our RNAseq analysis of TEC from *Hoil-1*$^{\Delta Foxn1}$ mice revealed heightened transcription of *Trp53* which, although required for TEC function (41), can also activate cell death and senescence (42). Future studies will reveal how LUBAC activity intersects with these pathways to impact TEC differentiation, survival and function.

Consistent with the subordinate role for SHARPIN in linear ubiquitination, thymi from *Sh*$^{cpdm/cpdm}$ mice exhibited milder TEC defects. Although there was a reduction in mTEC^{low} in *Sh*$^{cpdm/cpdm}$ mice compared to controls, all other major TEC subsets were normal. Thus, there appears to be sufficient LUBAC activity in SHARPIN-deficient TEC to support near normal thymic function and homeostasis. Since compound loss of TNF or Caspase-8 plus RIPK3 or Caspase-8 and MLKL did not restore the mTEC^{low} compartment of *Sh*$^{cpdm/cpdm}$ mice, we conclude that the reduced LUBAC activity in *Sh*$^{cpdm/cpdm}$ mice did not predispose these TECs to cell death. Rather, it is likely that SHARPIN is required for the optimal transduction of NF-κB signaling, perhaps downstream of CD40/CD40L interactions, which have previously been shown to mediate mTEC^{low} survival and/or expansion (7, 30).

In conclusion, this study defines differential roles for LUBAC components in TECs that correlate with their function in linear ubiquitination. These data reveal dual roles for LUBAC in the development and maintenance of the thymic microenvironment.

Methods

Mice

The *Sharpin*$^{cpdm/cpdm}$ mutant mouse strain arose on a C57BL/6/Ka background (26) and these mice were backcrossed twice onto a C57BL/6 background (22). The *Foxn1*^{cre}, *Rnf31*^{lox}, *Rbck1*^{lox}, *Sh*$^{cpdm/cpdm}$*TNF*$^{-/-}$, *Sh*$^{cpdm/cpdm}$*Casp8*$^{-/-}$*Mlkl*$^{-/-}$ and *Sh*$^{cpdm/cpdm}$*Casp8*$^{+/-}$*Ripk3*$^{-/-}$ were generated as previously described (20, 22, 25, 43) and were maintained on a C57BL/6 background. No randomisation or blinding of animals was performed for experiments. All mice were housed under specific pathogen-free housing conditions according to the regulations of the Walter and Eliza Hall Institute of Medical Research.

Thymus digestion

This procedure is described in detail elsewhere (44); briefly, the two thymic lobes were separated and connective tissue was removed with forceps. Snips were made in each lobe with surgical scissors and the fragments were agitated in 5 mL of RPMI-1640 medium with 25.96 mM HEPES with a wide-bore pipette tip. The supernatant was recovered and replaced by 1 mL of digestion buffer (RPMI-HEPES supplemented with 0.5 Wunsch units Liberase TM (Roche) and DNase I at 0.1% (w/v) (Sigma-Aldrich)). Thymic tissue was then digested at 37ºC for 15 min with gentle agitation after every 5 min. The supernatant was then replaced with 500 µL of digestion buffer and the digestion incubation was repeated for 15 min. The single cell suspensions recovered as Fractions 1 and 2 were stained with antibodies to analyze TEC phenotype and number.

Flow cytometry

Single-cell suspensions of lymphoid tissue were stained with various fluorochrome-conjugated antibodies. Surface staining of TECs was performed using the following antibodies that were made at The Walter and Eliza Hall Institute, unless otherwise stated. The TEC lineage depletion cocktail consisted of antibodies against mouse CD16/32 (FcgR-block, clone 2.4G2), mouse CD45 PerCP/Cy5.5 (clone 30-F11, Biolegend), mouse CD31 PerCP/Cy5.5 (clone 390, Biolegend) and mouse TER119 PerCP/Cy5.5 (clone TER119, Biolegend). Other conjugates included antibodies to mouse CD326 (EpCAM) APC/Cy7 (clone G8.8, Biolegend), H2-A/E FITC or APC (clone M5/114.15.2), H2-A/E BV421 (clone M5/114.15.2, Biolegend), biotinylated UEA-1 lectin (Vector labs, USA), mouse Ly51 PE or FITC (clone 6C3, Biolegend) and CD80 BV421 (clone 16-10A1, Biolegend). Second step staining with streptavidin PE/Cy7 (BD Biosciences, USA) was used to detect biotinylated UEA1 (Vector Laboratories). Propidium iodide (PI) or DAPI at a final concentration of 2.5 μg/mL was added to unfixed samples just prior to data acquisition to label dead cells. Intracellular staining with antibodies against human Ki67 FITC (clone MOPC-21, BD Pharmingen) and mouse AIRE FITC (clone 5H12) was performed after fixation and permeabilization using the FoxP3 detection kit (eBioscience). Lymphocytes were stained using antibodies of the following specificities: mouse TCRβ PE/Cy7 (H57.59.1, Biolegend), mouse CD4 APC (clone H129), mouse CD4 PerCP/Cy5.5 (GK1.5, Biolegend), mouse CD8 APC/Cy7 or BV650 (clone 53-6.7, Biolegend), mouse CD25 PE or BV510 (clone PC61, Biolegend), mouse CD44 PE or FITC (clone IM781), mouse CD122 PE (clone TM-β1), mouse CD62L APC/Cy7 (clone MEL-14, Biolegend) and mouse FOXP3 eFluor-450 (clone FJK-165, eBioscience). The immature thymocyte depletion cocktail contained biotinylated antibodies against mouse NK1.1 (clone PK136, Biolegend), TER119 (TER119), GR1 (clone RB6-8C5), Mac-1 (clone M1-170) and B220 (RA3-6B2), and they were detected with streptavidin BV786 (Biolegend). Screening of

TCRVβ repertoire in the $CD4^+$ and $CD8^+$ populations was performed with the mouse Vβ TCR Screening Panel (BD Pharmingen). Samples were acquired using Fortessa X20 (BD Biosciences) and LSR II analysers (BD Bioscience) and data analyzed using FlowJo software 9.9 (TreeStar).

PCR

The floxed allele (in the absence of Cre) in sorted TECs ($CD45^-MHCII^+EpCAM^+$), stromal cells ($CD45^-EpCAM^-$) and hematopoietic cells ($CD45^+EpCAM^-$) from 3-4 week-old *Hoil-1*$^{lox/lox}$ and *Hoil-1*$^{\Delta Foxn1}$ mice was detected by using *Hoil-1*-Fwd 5'-ACC CTA GGC CTA GTC AGT GCA AA-3' with *Hoil-1*-Rev-5'-AGG CTG TGG TCC ATT CTA GCC AT-3' producing 580bp band. The conditions were: 96 ºC 2 min; 30 cycles for 96 ºC 20 s, 57 ºC 20 s, 72 ºC 1 min 20 s and final extension of 72 ºC 5 min. The deleted allele (after Cre-mediated recombination) was detected by using Fwd 5'- ATG GTC TAC AGA AGA AAA CAG GC-3' and Rev 5'-GGG AGA TTC AGA CAA GGT TTC-3' producing 581bp. The conditions were: 94ºC 4 min; 30 cycles for 94ºC 40 s, 55ºC 30 s, 72ºC 1 min and final extension of 72ºC 5 min.

Immunohistology

Thymi from adult (8 weeks) and neonatal (day 4) mice were isolated, embedded in Tissue-Tek O.C.T compound (Sakura Finetek, U.S.A.) and snap frozen in a liquid nitrogen/isopentane slurry. Sections of 5-8μm were cut using a Microm HM550 Cryostat (Thermo Scientific). Sections were fixed in ice cold acetone (Merck) for 3 min and air-dried for 2 min. Sections were blocked with 5% (v/v) goat serum in PBS with 0.1% Tween-20 (v/v) for 30 min at room temperature before incubation with primary antibodies for 30 min. Primary antibodies of the following specificities were used: mouse K5 (Covance, clone Poly 19055), biotinylated mouse pan-keratin (LifeSpan BioSciences, clone Lu-5), biotinylated UEA-1 lectin (Vector labs, USA), mouse AIRE-Alexa647

(clone 5H12), mouse K8 (clone Troma-I, DSHB) and ER-TR7 (provided by Prof Richard Boyd, Monash University). Following three 5 min washes in PBS, sections were incubated with appropriate secondary reagents (antibodies or streptavidin) conjugated to fluorochromes (anti-rabbit IgG Alexa-555 (Life Technologies) and streptavidin FITC (Invitrogen)) for 30 min, counterstained with DAPI (Sigma-Aldrich), then mounted with Vectashield (Vector labs). Images were collected using a LSM780 confocal microscope with Zen 2012 SP2 (black) software v11.0 (Zeiss). Single optical sections and maximal intensity projection images were processed for presentation using OMERO (45) or ImageJ (2.0.0). For quantification of medullary area, 1 of 40 neighbouring sections, or every 1 of 20 for thymic from adult *Hoil-1*$^{\Delta Foxn1}$ mice, were selected as a representative section, stained with UEA-1(40) and processed using ImageJ (2.0.0).

RNA sequencing

Thymi were pooled from 8- or 2-week-old WT mice and digested to isolate TECs ($CD45^-$ $MHCII^+EpCAM^+$) (44). At the end of the digestion, fractions were pooled, enriched and purified using anti-mouse CD45 microbeads (Miltenyi Biotec, Germany, Cat # 130052301) and FACS ARIA (BD). Cell pellets were snap frozen on dry ice and stored at -80°C. RNA was isolated using the miRNeasy Micro Kit (Qiagen) with on column DNase digestion according to manufacturer's instructions. First strand cDNA synthesis and cDNA amplification were performed using the SMART-Seq® v4 Ultra® Low Input RNA Kit for Sequencing (Clontech Laboratories) according to manufacturer's instructions. Complementary DNA (cDNA) libraries were prepared and indexed separately using the Nextera® XT DNA Library Preparation Kit (Illumina) following manufacturer's instructions. Each indexed cDNA sample library was quantified using the Agilent TAPE station and the Qubit™ DNA BR assay kit for Qubit 3.0® Fluorometer (Life technologies).

The indexed sample libraries were pooled and diluted to 1.5pM for 75 base paired-end sequencing on a NextSeq 500 instrument using the v2 150 cycle High Output kit (Illumina) according to the manufacturer's instructions.

Between 13 and 35 million read pairs were generated for each sample and reads were aligned to the Mus musculus genome (mm10) using Rsubread (46). The number of read pairs overlapping mouse Entrez genes was summarized using featureCounts and Rsubread's built-in NCBI gene annotation. Low expressed genes were filtered out using edgeR's filterByExpr function (47). Genes without current annotation were also filtered. Differential expression (DE) analyses were undertaken using the edgeR and limma (48) software packages. Library sizes were normalized using the trimmed mean of M-values (TMM) method (49). Sample quality weights were estimated using voomWithQualityWeights (50)and differential expression was evaluated using voom (51) with robust empirical Bayes estimation of the variances (52). Correlations between repeated measurements from the same mouse were estimated using the duplicateCorrelation method (53). The false discovery rate (FDR) was controlled below 0.05 using the method of Benjamini and Hochberg. Over-representation of Gene Ontology (GO) terms and KEGG pathways for the differentially expressed genes were identified using limma's goana and kegga functions. Barcode plots illustrating the cross correlations between the cell types, and enrichment of interested pathway genes were drawn using limma's barcodeplot function. Gene set enrichment tests used the roast method (54). Heatmaps were drawn using limma's coolmap function. Sequence data that support the findings of this study have been deposited with GEO with the primary accession code GSE139898.

Hematopoietic reconstitution experiments

Bone marrow reconstitution experiments were performed using recipient WT (C57BL/6-Ly5.1) mice irradiated with 2x 550 RAD and reconstituted within 24 hours by intravenous injection with $5X10^6$ of BM cells from donors of interest (all on a C57BL/6-Ly5.2 background). Reconstituted mice were analyzed 6.5 weeks after reconstitution.

Data analysis

Statistical analyses were performed using Prism version 7. Experiments containing three or more groups were analyzed using ANOVA followed by a Tukey's post-hoc test. Experiments with two groups were analyzed with two-tailed Student's t-test. P-values <0.05 were considered as the threshold for statistical significance for all statistical tests.

Author contributions

Conceptualization, R.J., A.S. and D.H.D.G.; Methodology, R.J., J.M.S., A.S. and D.H.D.G.; Investigation, R.J., J.M.S., M.H., K.Z., F.K. and D.H.D.G.; Resources, P.B., C.H., J.R., H.W., J.S., A.S., D.H.D.G.; Writing - Original draft, R.J., J.M.S., and D.H.D.G.; Writing – Review and editing, R.J., J.M.S., M.H., K.Z., A.S., H.W., J.S. and D.H.D.G. The authors declare no conflict of interest. Correspondence and requests for materials should be addressed to D.H.D.G. (dgray@wehi.edu.au).

Acknowledgments

We gratefully acknowledge the Gray, Strasser and Herold laboratories and Dr Nieves Peltzer for valuable feedback on this study. We thank the WEHI Flow Cytometry Laboratory and the Centre for Dynamic Imaging; B Helbert, K Mackwell, C Young for mouse genotyping; G Siciliano, H

Marks, K Humphreys and S O'Connor for animal husbandry; and L Tai for technical assistance. TROMA-I was deposited to the DSHB by Brulet, P./Kemler, R. (DSHB Hybridoma Product TROMA-I). This work was supported by grants GNT0637353, GNT1049724 and GNT1121325 and Career Development Fellowship-2 1090236 (for D.H.D.G.), 1016701, Senior Principal Research Fellow [SPRF] Fellowship 1020363 (for A.S) from the Australian National Health and Medical Research Council and the Leukaemia Research Foundation. R.J. was supported by MIRS and MIFRS from the University of Melbourne. H.W. is supported by an Alexander von Humboldt Professorship Award, a Wellcome Trust Investigator Award (214342/Z/18/Z), a Cancer Research UK programme grant (A27323), a Medical Research Council UK Grant (MR/S00811X/1) and by the German Research Foundation (DFG) in the context of SFB 1399 and SFB 1403. This work was made possible through Victorian State Government Operational Infrastructure Support and Australian Government NHMRC IRIISS. The authors have no conflicting financial interests.

References

1. Petrie HT, Zuniga-Pflucker JC. Zoned out: functional mapping of stromal signaling microenvironments in the thymus. Annu Rev Immunol. 2007;25:649-79.

2. Klein L, Kyewski B, Allen PM, Hogquist KA. Positive and negative selection of the T cell repertoire: what thymocytes see (and don't see). Nat Rev Immunol. 2014;14(6):377-91.

3. Takaba H, Morishita Y, Tomofuji Y, Danks L, Nitta T, Komatsu N, et al. Fezf2 Orchestrates a Thymic Program of Self-Antigen Expression for Immune Tolerance. Cell. 2015;163(4):975-87.

4. Abramson J, Anderson G. Thymic Epithelial Cells. Annu Rev Immunol. 2017;35:85-118.

5. Cosway EJ, Lucas B, James KD, Parnell SM, Carvalho-Gaspar M, White AJ, et al. Redefining thymus medulla specialization for central tolerance. J Exp Med. 2017.

6. Sun SC. The non-canonical NF-kappaB pathway in immunity and inflammation. Nat Rev Immunol. 2017.

7. Akiyama T, Shimo Y, Yanai H, Qin J, Ohshima D, Maruyama Y, et al. The tumor necrosis factor family receptors RANK and CD40 cooperatively establish the thymic medullary microenvironment and self-tolerance. Immunity. 2008;29(3):423-37.

8. Desanti GE, Cowan JE, Baik S, Parnell SM, White AJ, Penninger JM, et al. Developmentally regulated availability of RANKL and CD40 ligand reveals distinct mechanisms of fetal and adult cross-talk in the thymus medulla. J Immunol. 2012;189(12):5519-26.

9. Hikosaka Y, Nitta T, Ohigashi I, Yano K, Ishimaru N, Hayashi Y, et al. The cytokine RANKL produced by positively selected thymocytes fosters medullary thymic epithelial cells that express autoimmune regulator. Immunity. 2008;29(3):438-50.

530 10. Gerlach B, Cordier SM, Schmukle AC, Emmerich CH, Rieser E, Haas TL, et al. Linear
531 ubiquitination prevents inflammation and regulates immune signalling. Nature.
532 2011;471(7340):591-6.
533 11. Haas TL, Emmerich CH, Gerlach B, Schmukle AC, Cordier SM, Rieser E, et al.
534 Recruitment of the linear ubiquitin chain assembly complex stabilizes the TNF-R1 signaling
535 complex and is required for TNF-mediated gene induction. Mol Cell. 2009;36(5):831-44.
536 12. Tokunaga F, Nakagawa T, Nakahara M, Saeki Y, Taniguchi M, Sakata S, et al. SHARPIN
537 is a component of the NF-kappaB-activating linear ubiquitin chain assembly complex. Nature.
538 2011;471(7340):633-6.
539 13. Draber P, Kupka S, Reichert M, Draberova H, Lafont E, de Miguel D, et al. LUBAC-
540 Recruited CYLD and A20 Regulate Gene Activation and Cell Death by Exerting Opposing Effects
541 on Linear Ubiquitin in Signaling Complexes. Cell Rep. 2015;13(10):2258-72.
542 14. Ikeda F, Deribe YL, Skanland SS, Stieglitz B, Grabbe C, Franz-Wachtel M, et al.
543 SHARPIN forms a linear ubiquitin ligase complex regulating NF-kappaB activity and apoptosis.
544 Nature. 2011;471(7340):637-41.
545 15. Kirisako T, Kamei K, Murata S, Kato M, Fukumoto H, Kanie M, et al. A ubiquitin ligase
546 complex assembles linear polyubiquitin chains. EMBO J. 2006;25(20):4877-87.
547 16. Yamanaka K, Ishikawa H, Megumi Y, Tokunaga F, Kanie M, Rouault TA, et al.
548 Identification of the ubiquitin-protein ligase that recognizes oxidized IRP2. Nat Cell Biol.
549 2003;5(4):336-40.
550 17. Boisson B, Laplantine E, Dobbs K, Cobat A, Tarantino N, Hazen M, et al. Human HOIP
551 and LUBAC deficiency underlies autoinflammation, immunodeficiency, amylopectinosis, and
552 lymphangiectasia. J Exp Med. 2015;212(6):939-51.

18. Boisson B, Laplantine E, Prando C, Giliani S, Israelsson E, Xu Z, et al. Immunodeficiency, autoinflammation and amylopectinosis in humans with inherited HOIL-1 and LUBAC deficiency. Nat Immunol. 2012;13(12):1178-86.

19. Liang Y, Seymour RE, Sundberg JP. Inhibition of NF-kappaB signaling retards eosinophilic dermatitis in SHARPIN-deficient mice. J Invest Dermatol. 2011;131(1):141-9.

20. Teh CE, Lalaoui N, Jain R, Policheni AN, Heinlein M, Alvarez-Diaz S, et al. Linear ubiquitin chain assembly complex coordinates late thymic T-cell differentiation and regulatory T-cell homeostasis. Nat Commun. 2016;7:13353.

21. Peltzer N, Darding M, Montinaro A, Draber P, Draberova H, Kupka S, et al. LUBAC is essential for embryogenesis by preventing cell death and enabling haematopoiesis. Nature. 2018;557(7703):112-7.

22. Rickard JA, Anderton H, Etemadi N, Nachbur U, Darding M, Peltzer N, et al. TNFR1-dependent cell death drives inflammation in Sharpin-deficient mice. Elife. 2014;3.

23. Kumari S, Redouane Y, Lopez-Mosqueda J, Shiraishi R, Romanowska M, Lutzmayer S, et al. Sharpin prevents skin inflammation by inhibiting TNFR1-induced keratinocyte apoptosis. Elife. 2014;3.

24. Lafont E, Draber P, Rieser E, Reichert M, Kupka S, de Miguel D, et al. TBK1 and IKKepsilon prevent TNF-induced cell death by RIPK1 phosphorylation. Nat Cell Biol. 2018;20(12):1389-99.

25. Peltzer N, Rieser E, Taraborrelli L, Draber P, Darding M, Pernaute B, et al. HOIP deficiency causes embryonic lethality by aberrant TNFR1-mediated endothelial cell death. Cell Rep. 2014;9(1):153-65.

575 26. HogenEsch H, Gijbels MJ, Offerman E, van Hooft J, van Bekkum DW, Zurcher C. A
576 spontaneous mutation characterized by chronic proliferative dermatitis in C57BL mice. Am J
577 Pathol. 1993;143(3):972-82.
578 27. Seymour RE, Hasham MG, Cox GA, Shultz LD, Hogenesch H, Roopenian DC, et al.
579 Spontaneous mutations in the mouse Sharpin gene result in multiorgan inflammation, immune
580 system dysregulation and dermatitis. Genes Immun. 2007;8(5):416-21.
581 28. Park Y, Jin HS, Lopez J, Lee J, Liao L, Elly C, et al. SHARPIN controls regulatory T cells
582 by negatively modulating the T cell antigen receptor complex. Nat Immunol. 2016;17(3):286-96.
583 29. Webb LV, Barbarulo A, Huysentruyt J, Vanden Berghe T, Takahashi N, Ley S, et al.
584 Survival of Single Positive Thymocytes Depends upon Developmental Control of RIPK1 Kinase
585 Signaling by the IKK Complex Independent of NF-kappaB. Immunity. 2019;50(2):348-61 e4.
586 30. Gray DH, Seach N, Ueno T, Milton MK, Liston A, Lew AM, et al. Developmental kinetics,
587 turnover, and stimulatory capacity of thymic epithelial cells. Blood. 2006;108(12):3777-85.
588 31. Williams JA, Zhang J, Jeon H, Nitta T, Ohigashi I, Klug D, et al. Thymic medullary
589 epithelium and thymocyte self-tolerance require cooperation between CD28-CD80/86 and CD40-
590 CD40L costimulatory pathways. J Immunol. 2014;192(2):630-40.
591 32. den Braber I, Mugwagwa T, Vrisekoop N, Westera L, Mogling R, de Boer AB, et al.
592 Maintenance of peripheral naive T cells is sustained by thymus output in mice but not humans.
593 Immunity. 2012;36(2):288-97.
594 33. Venables T, Griffith AV, DeAraujo A, Petrie HT. Dynamic changes in epithelial cell
595 morphology control thymic organ size during atrophy and regeneration. Nat Commun.
596 2019;10(1):4402.

34. Taraborrelli L, Peltzer N, Montinaro A, Kupka S, Rieser E, Hartwig T, et al. LUBAC prevents lethal dermatitis by inhibiting cell death induced by TNF, TRAIL and CD95L. Nat Commun. 2018;9(1):3910.

35. Alvarez-Diaz S, Dillon CP, Lalaoui N, Tanzer MC, Rodriguez DA, Lin A, et al. The Pseudokinase MLKL and the Kinase RIPK3 Have Distinct Roles in Autoimmune Disease Caused by Loss of Death-Receptor-Induced Apoptosis. Immunity. 2016;45(3):513-26.

36. Peltzer N, Walczak H. Cell Death and Inflammation - A Vital but Dangerous Liaison. Trends Immunol. 2019;40(5):387-402.

37. Jenkinson SR, Williams JA, Jeon H, Zhang J, Nitta T, Ohigashi I, et al. TRAF3 enforces the requirement for T cell cross-talk in thymic medullary epithelial development. Proc Natl Acad Sci U S A. 2013;110(52):21107-12.

38. Shen H, Ji Y, Xiong Y, Kim H, Zhong X, Jin MG, et al. Medullary thymic epithelial NF-kB-inducing kinase (NIK)/IKKalpha pathway shapes autoimmunity and liver and lung homeostasis in mice. Proc Natl Acad Sci U S A. 2019;116(38):19090-7.

39. Shimizu Y, Taraborrelli L, Walczak H. Linear ubiquitination in immunity. Immunol Rev. 2015;266(1):190-207.

40. Sakata M, Ohigashi I, Takahama Y. Cellularity of Thymic Epithelial Cells in the Postnatal Mouse. J Immunol. 2018;200(4):1382-8.

41. Rodrigues PM, Ribeiro AR, Perrod C, Landry JJM, Araujo L, Pereira-Castro I, et al. Thymic epithelial cells require p53 to support their long-term function in thymopoiesis in mice. Blood. 2017;130(4):478-88.

42. Aubrey BJ, Kelly GL, Janic A, Herold MJ, Strasser A. How does p53 induce apoptosis and how does this relate to p53-mediated tumour suppression? Cell Death Differ. 2018;25(1):104-13.

620 43. Zuklys S, Gill J, Keller MP, Hauri-Hohl M, Zhanybekova S, Balciunaite G, et al. Stabilized
621 beta-catenin in thymic epithelial cells blocks thymus development and function. J Immunol.
622 2009;182(5):2997-3007.
623 44. Jain R, Gray DH. Isolation of thymic epithelial cells and analysis by flow cytometry. Curr
624 Protoc Immunol. 2014;107:3 26 1-15.
625 45. Allan C, Burel JM, Moore J, Blackburn C, Linkert M, Loynton S, et al. OMERO: flexible,
626 model-driven data management for experimental biology. Nat Methods. 2012;9(3):245-53.
627 46. Liao Y, Smyth GK, Shi W. The R package Rsubread is easier, faster, cheaper and better
628 for alignment and quantification of RNA sequencing reads. Nucleic Acids Res. 2019;47(8):e47.
629 47. Chen Y, Lun AT, Smyth GK. From reads to genes to pathways: differential expression
630 analysis of RNA-Seq experiments using Rsubread and the edgeR quasi-likelihood pipeline.
631 F1000Res. 2016;5:1438.
632 48. Ritchie ME, Phipson B, Wu D, Hu Y, Law CW, Shi W, et al. limma powers differential
633 expression analyses for RNA-sequencing and microarray studies. Nucleic Acids Res.
634 2015;43(7):e47.
635 49. Robinson MD, Oshlack A. A scaling normalization method for differential expression
636 analysis of RNA-seq data. Genome Biol. 2010;11(3):R25.
637 50. Liu R, Holik AZ, Su S, Jansz N, Chen K, Leong HS, et al. Why weight? Modelling sample
638 and observational level variability improves power in RNA-seq analyses. Nucleic Acids Res.
639 2015;43(15):e97.
640 51. Law CW, Chen Y, Shi W, Smyth GK. voom: Precision weights unlock linear model
641 analysis tools for RNA-seq read counts. Genome Biol. 2014;15(2):R29.

642 52. Phipson B, Lee S, Majewski IJ, Alexander WS, Smyth GK. Robust Hyperparameter
643 Estimation Protects against Hypervariable Genes and Improves Power to Detect Differential
644 Expression. Ann Appl Stat. 2016;10(2):946-63.
645 53. Smyth GK, Michaud J, Scott HS. Use of within-array replicate spots for assessing
646 differential expression in microarray experiments. Bioinformatics. 2005;21(9):2067-75.
647 54. Wu D, Lim E, Vaillant F, Asselin-Labat ML, Visvader JE, Smyth GK. ROAST: rotation
648 gene set tests for complex microarray experiments. Bioinformatics. 2010;26(17):2176-82.
649

Figure Legends

Figure 1: Early thymic atrophy and T cell defects in *Hoil-1$^{\Delta Foxn1}$* and *Hoip$^{\Delta Foxn1}$* mice

(**A**) RNA-seq expression analysis of LUBAC components from cTECs, mTEC^{hi} and mTEC^{low} from 8-week-old WT mice. (**B**) Thymic cellularity of 8-week-old *Hoil-1$^{\Delta Foxn1}$* or *Hoip$^{\Delta Foxn1}$*, 6-week-old *Sh$^{cpdm/cpdm}$*, mice versus controls. (**C**) Flow cytometry plots of thymocyte CD4 vs. CD8 expression from 8-week-old *Hoil-1$^{\Delta Foxn1}$* mice and *Hoil-1$^{lox/lox}$* controls, with cell numbers quantified (left panel). (**D**) Thymocyte subset numbers in 3-week-old *Hoip$^{lox/lox}$* and *Hoip$^{\Delta Foxn1}$* mice. (**E**) Numbers of splenic TCRβ^{+}CD4^{+} and TCRβ^{+}CD8^{+} T cells from 8-week-old *Hoil-1$^{\Delta Foxn1}$* and *Hoil-1$^{lox/lox}$* mice. (**F**) Flow cytometry plots of CD44 vs. CD62L expression gated on splenic TCRβ^{+}CD4^{+} or TCRβ^{+}CD8^{+} T cells from 8-week-old *Hoil-1$^{\Delta Foxn1}$* mice and *Hoil-1$^{lox/lox}$* controls. Graphs show the numbers of naïve (CD44^{low}/CD62L^{high}), effector (CD44^{high}/CD62L^{low}) and central memory (CD44^{high}/CD62L^{high}) T cells. (**G**) Thymic cellularity of control and *Hoil-1$^{\Delta Foxn1}$* mice at the indicated ages. The numbers in parentheses indicate the mean fold-change in thymic cellularity (controls vs *Hoil-1$^{\Delta Foxn1}$* mice). All data are representative of at least two independent experiments shown (except **A**) (n≥3/group). Graphs show mean ± SEM and groups were compared with a Student's t test (two-sided, unpaired). * $p<0.05$, ** $p<0.01$; *** $p<0.001$; **** $p<0.0001$.

Figure 2: Loss of TECs and severe disruption of thymic architecture in *Hoil-1$^{\Delta Foxn1}$* and *Hoip$^{\Delta Foxn1}$* mice.

TEC (CD45$^-$MHCII$^+$EpCAM$^+$) number from **(A)** 13-week-old *Hoil-1$^{lox/lox}$* and *Hoil-1$^{\Delta Foxn1}$* mice or **(B)** 13-week-old *Hoip$^{lox/lox}$* and *Hoip$^{\Delta Foxn1}$* mice. Representative flow cytometry plots gated on TECs from **(C)** 13-week-old *Hoil-1$^{lox/lox}$* and *Hoil-1$^{\Delta Foxn1}$* mice or **(D)** 13-week-old *Hoip$^{lox/lox}$* and *Hoip$^{\Delta Foxn1}$* mice showing Ly51 vs. UEA-1 expression. (**E, F**) Mean proportion and number of cTECs (Ly51$^+$UEA-1$^-$), mTECs (Ly51$^-$UEA-1$^+$) or "double negative" TECs (Ly51$^-$UEA-1$^-$) from **(E)** 13-week-old *Hoil-1$^{lox/lox}$* and *Hoil-1$^{\Delta Foxn1}$* mice or **(F)** 13-week-old *Hoip$^{lox/lox}$* and *Hoip$^{\Delta Foxn1}$* mice. **(G-L)** Immunofluorescence images of thymic sections from 8-9-week-old *Hoil-1$^{lox/lox}$*, *Hoil-1$^{\Delta Foxn1}$, Hoip$^{lox/lox}$* and *Hoip$^{\Delta Foxn1}$* mice stained with anti-K8 and UEA-1 **(G, J)**, anti-K5 and anti-AIRE **(H, K)** and ER-TR7 and anti-PanK **(I, L)**. Scale bars represent 200 μm **(G, I, J, L)** and 20 μm **(H, K).** * and ** represents epithelial-cell free regions. Data are representative of at least two independent experiments (n≥ 3/group). Graph bars indicate mean ± SEM and groups were compared with a Student's t test (two sided, unpaired). * $p<0.05$; ** $p<0.01$; *** $p<0.001$; **** $p<0.0001$.

Figure 3: HOIL-1 deficiency induces early loss of mTECs in *Hoil-1$^{\Delta Foxn1}$* mice.

(A) TEC (CD45$^-$MHCII$^+$EpCAM$^+$) numbers from E15.5 or 4-day-old *Hoil-1$^{lox/lox}$* and *Hoil-1$^{\Delta Foxn1}$* mice. **(B)** Representative flow cytometry plots from thymic digests from individual E15.5 or 4-day-old *Hoil-1$^{lox/lox}$* and *Hoil-1$^{\Delta Foxn1}$* mice showing Ly51 vs. UEA-1 gated on TECs (left and middle panels) and CD80 vs. UEA-1 gated on mTECs (right panels). Graphs showing mean proportions (top; of total TEC) and absolute numbers (bottom) of cTECs (Ly51$^+$UEA-1$^-$) and total mTECs (Ly51$^-$UEA-1$^+$) from E15.5 (**C**) or cTECs, CD80^{hi} mTECs and CD80$^{lo/-}$ mTECs from 4-day-old (**D**) *Hoil-1$^{lox/lox}$* and *Hoil-1$^{\Delta Foxn1}$* mice. (**E**) Representative flow cytometry plots of MHC II vs AIRE expression gated on CD80^{hi} mTECs from 4-day-old *Hoil-1$^{lox/lox}$* and *Hoil-1$^{\Delta Foxn1}$* mice and mean cell numbers. **(F)** Representative histograms and **(G)** graphs showing proportions of proliferating Ki67$^+$ TECs. **(H-J)** Immunofluorescence images of thymic sections from 4-day-old *Hoil-1$^{lox/lox}$* and *Hoil-1$^{\Delta Foxn1}$* mice stained with anti-K8 and UEA-1 **(H)**, anti-K5 and AIRE **(I)** and ER-TR7 and anti-PanK **(J)**. Scale bars represent 200 μm **(H, J)** and 20 μm **(I)**. Graph bars indicate mean ± SEM and experiments with two groups were compared with a Student's t test (two sided, unpaired)

Figure 4: HOIL-1 is required to prevent TEC cell death

(A) Multidimensional scaling (MDS) plot of RNAseq data from purified cTECs and mTEC^{hi} from 2-week-old *Hoil-1$^{lox/lox}$* and *Hoil-1$^{\Delta Foxn1}$* mice, taking into account the top 500 most variable genes between a given two samples. **(B)** Plots of the log-fold changes (*Hoil-1$^{\Delta Foxn1}$*/*Hoil-1$^{lox/lox}$*) vs average expression for all genes in cTECs (top) and mTEC^{hi} (bottom). Those genes that are significantly upregulated (red) or downregulated (blue) in cell subsets from *Hoil-1*$^{\Delta Foxn1}$ mice when compared to *Hoil-1*$^{lox/lox}$ control mice are highlighted. **(C)** Heatmaps showing the expression of genes involved in necroptosis (GO:0070266) in purified mTEC^{hi} and cTEC subsets. **(D)** Graph of the mean thymic cellularity in 8-week-old *Hoil-1$^{\Delta Foxn1}$Casp8$^{-/-}$Mlkl$^{-/-}$* mice vs controls. **(E)** Graph of the proportions of T cells among splenocytes in *Hoil-1$^{\Delta Foxn1}$Casp8$^{-/-}$Mlkl$^{-/-}$* mice vs controls. **(F-H)** Graph of the total number of TECs (**F**), mTECs (**G**) or cTECs (**H**) recovered from 8-week-old *Hoil-1$^{\Delta Foxn1}$Casp8$^{-/-}$Mlkl$^{-/-}$* mice vs controls. Data are combined from three independent experiments (n≥1-3/group). Graph bars indicate mean ± SEM. **(I, J)** Immunofluorescence images of thymic sections from 8-week-old *Hoil-1$^{lox/lox}$* and *Hoil-1$^{\Delta Foxn1}$Casp8$^{-/-}$Mlkl$^{-/-}$* mice stained with anti-K8, anti-K5 and UEA-1 (scale bar = 200 μm).

Figure 5: SHARPIN is required for mTEC^{lo}.

(A) TEC (CD45^{-}MHCII^{+}EpCAM^{+}) numbers from 6-week-old controls and *cpdm* mice. **(B)** Representative flow cytometry plots and **(C)** graphs showing proportions and absolute numbers of mTEC^{hi} (MHCII^{hi}Ly51^{-}) and mTEC^{lo} mTECs (MHCII^{lo}Ly51^{-}) and cTECs (MHCII^{+}Ly51^{+}). Immunofluorescence images of thymic sections from 6-week-old *Sh*$^{cpdm/+}$ and *Sh*$^{cpdm/cpdm}$ mice stained with **(D)** anti-K8 and UEA-1, **(E)** anti-K5 and AIRE and **(F)** ER-TR7 and anti-PanK. Numbers of **(G)** TEC subsets in *Sh*$^{cpdm/cpdm}$, *Sh*$^{cpdm/cpdm}$*Casp8*$^{+/-}$*Ripk3*$^{-/-}$, *Sh*$^{cpdm/cpdm}$*Casp8*$^{-/-}$*Mlkl*$^{-/-}$, **(H)** *Sh*$^{cpdm/+}$*Tnf*$^{-/-}$, *Sh*$^{cpdm/cpdm}$*Tnf*$^{-/-}$. Graph bars indicate mean ± SEM and groups were compared with a Student's t test (two sided, unpaired). NS, not significant * $p<0.05$; ** $p<0.01$; *** $p<0.001$; **** $p<0.0001$. The control group combines various combinations of genotypes (*Sh*$^{+/+}$, *Sh*$^{cpdm/+}$; n≥ 3/group). Scale bars represent 100 μm **(D, F)** and 20 μm **(E)**.

Figure 1

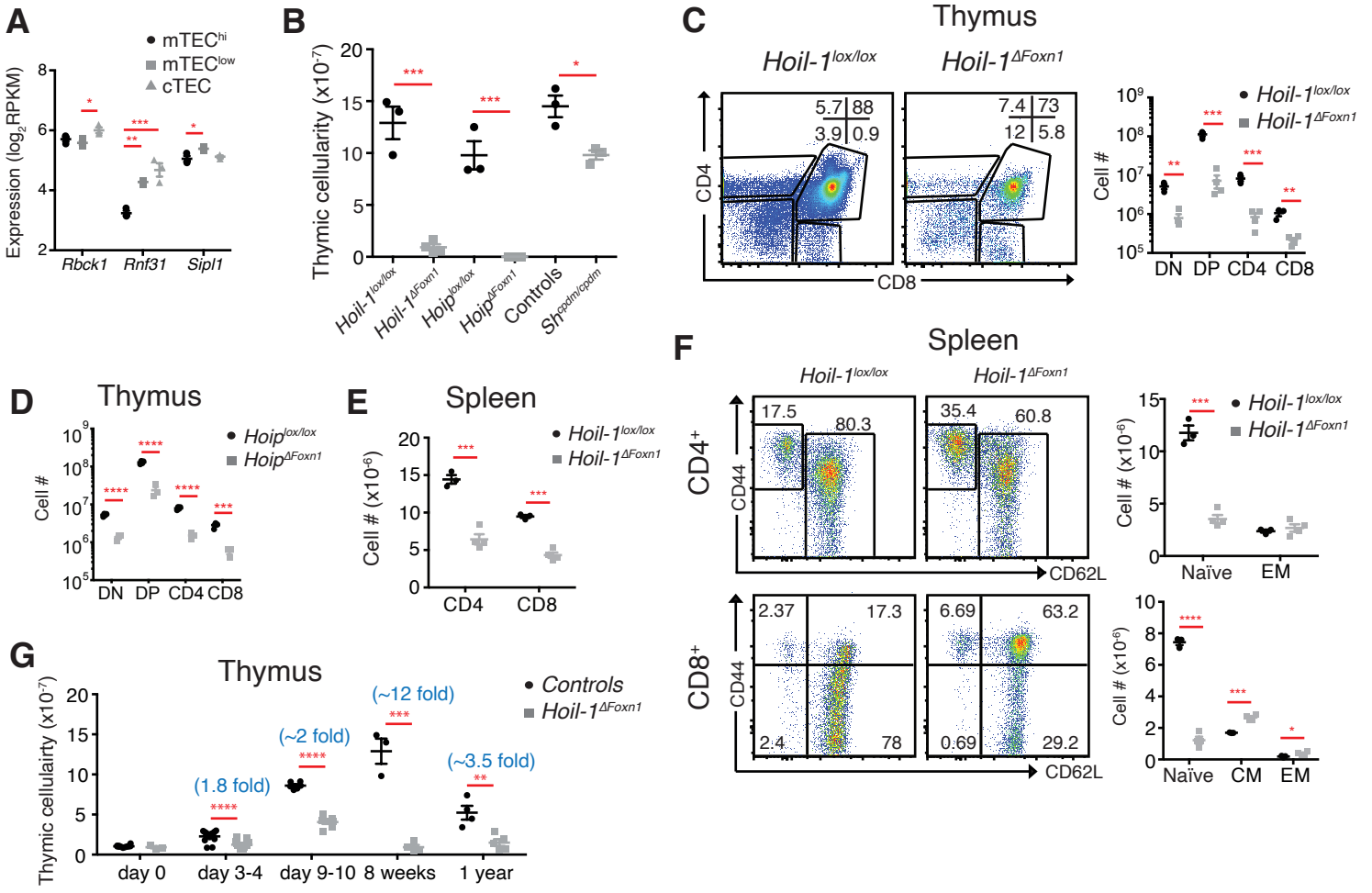
A
mTEC^hi
mTEC^low
cTEC
Expression (log2 RPKM)
Rbck1
Rnf31
Sipl1
B
Thymic cellularity (x10^-7)
Hoil-1^lox/lox
Hoil-1^ΔFoxn1
Hoip^lox/lox
Hoip^ΔFoxn1
Controls
Sh^cpdm/cpdm
C
Thymus
Hoil-1^lox/lox
Hoil-1^ΔFoxn1
5.7
88
3.9
0.9
7.4
73
12
5.8
CD4
CD8
Cell #
DN
DP
CD4
CD8
D
Thymus
Hoip^lox/lox
Hoip^ΔFoxn1
E
Spleen
Hoil-1^lox/lox
Hoil-1^ΔFoxn1
Cell # (x10^-6)
F
Spleen
CD4+
CD44
CD62L
17.5
80.3
35.4
60.8
Naïve
EM
CD8+
2.37
17.3
2.4
78
6.69
63.2
0.69
29.2
CM
G
Thymus
Controls
Hoil-1^ΔFoxn1
Thymic cellularity (x10^-7)
(1.8 fold)
(~2 fold)
(~12 fold)
(~3.5 fold)
day 0
day 3-4
day 9-10
8 weeks
1 year

Figure 2

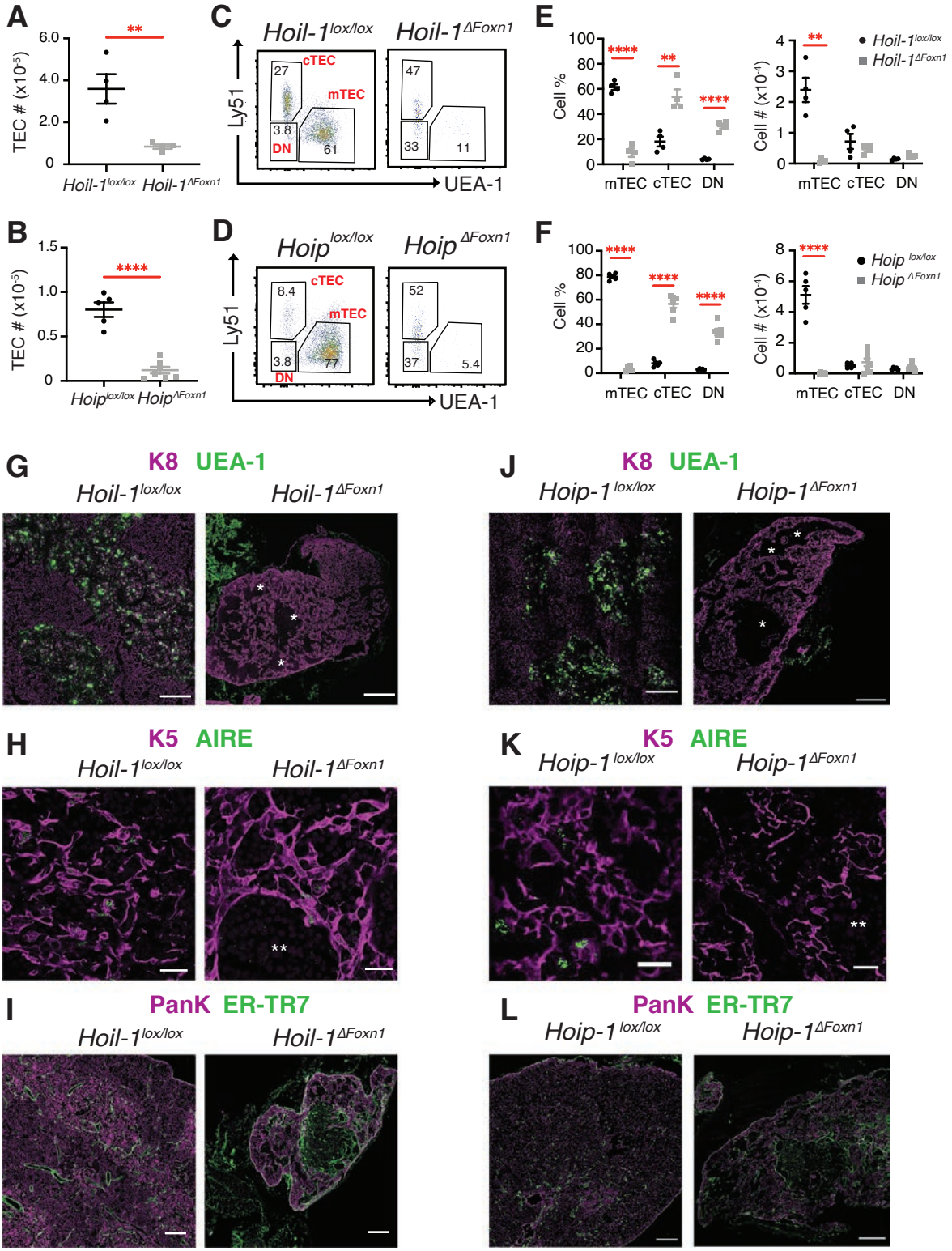
A
TEC # (x10⁻⁵)
Hoil-1lox/lox
Hoil-1ΔFoxn1
B
Hoip lox/lox
Hoip ΔFoxn1
C
Hoil-1lox/lox
Hoil-1ΔFoxn1
cTEC
mTEC
DN
Ly51
UEA-1
D
Hoip lox/lox
Hoip ΔFoxn1
E
Cell %
Cell # (x10⁻⁴)
mTEC cTEC DN
F
G
K8 UEA-1
H
K5 AIRE
I
PanK ER-TR7
J
Hoip-1 lox/lox
Hoip-1ΔFoxn1
K
L

Figure 3

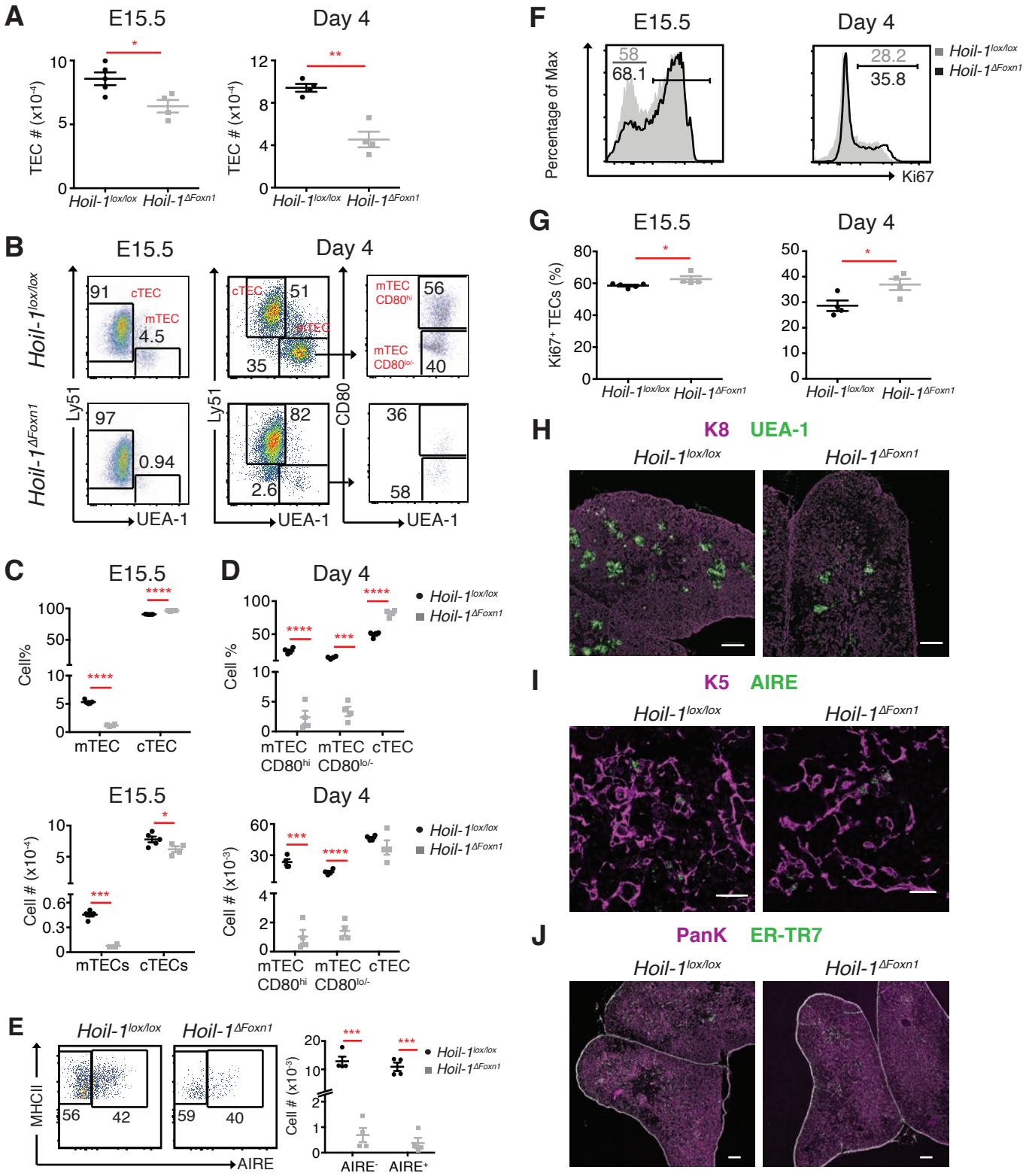
A
E15.5
Day 4
TEC # (x10⁻⁴)
Hoil-1lox/lox
Hoil-1ΔFoxn1
B
Hoil-1lox/lox
Hoil-1ΔFoxn1
cTEC
mTEC
Ly51
UEA-1
CD80
mTEC CD80hi
mTEC CD80lo/-
C
Cell%
mTEC
cTEC
D
Cell %
mTEC CD80hi
mTEC CD80lo/-
Cell # (x10⁻⁴)
Cell # (x10⁻³)
mTECs
cTECs
E
MHCII
AIRE
AIRE-
AIRE+
F
Percentage of Max
Ki67
G
Ki67+ TECs (%)
H
K8
UEA-1
I
K5
AIRE
J
PanK
ER-TR7

Figure 4

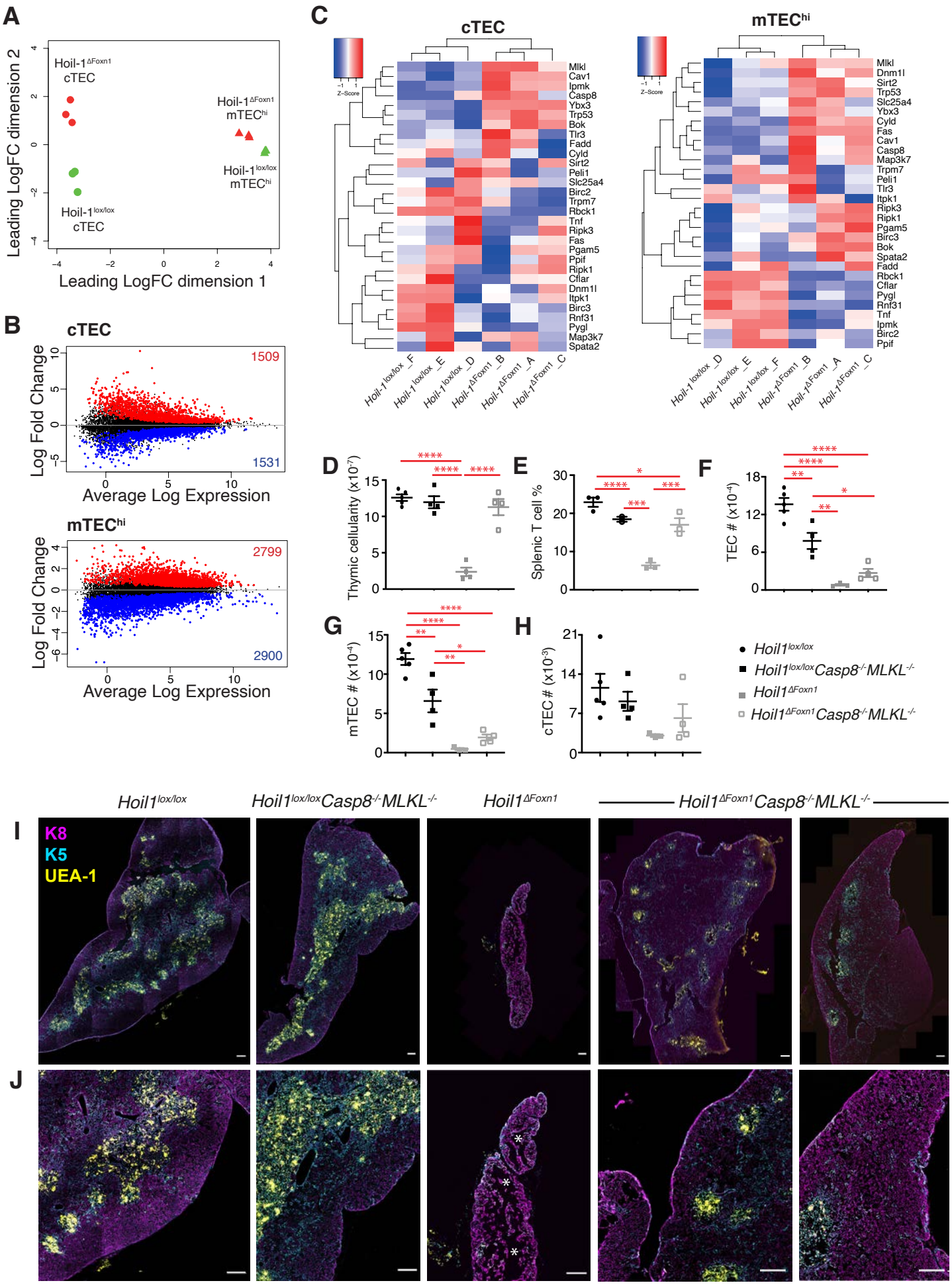
A
Hoil-1ΔFoxn1 cTEC
Hoil-1ΔFoxn1 mTEChi
Hoil-1lox/lox mTEChi
Hoil-1lox/lox cTEC
Leading LogFC dimension 2
Leading LogFC dimension 1
B
cTEC
1509
1531
Log Fold Change
Average Log Expression
mTEChi
2799
2900
C
cTEC
mTEChi
Z-Score
Mlkl
Cav1
Ipmk
Casp8
Ybx3
Trp53
Bok
Tlr3
Fadd
Cyld
Sirt2
Peli1
Slc25a4
Birc2
Trpm7
Rbck1
Tnf
Ripk3
Fas
Pgam5
Ppif
Ripk1
Cflar
Dnm1l
Itpk1
Birc3
Rnf31
Pygl
Map3k7
Spata2
Hoil-1lox/lox_F
Hoil-1lox/lox_E
Hoil-1lox/lox_D
Hoil-1ΔFoxn1_B
Hoil-1ΔFoxn1_A
Hoil-1ΔFoxn1_C
Hoil-1lox/lox_D
Hoil-1lox/lox_E
Hoil-1lox/lox_F
Hoil-1ΔFoxn1_B
Hoil-1ΔFoxn1_A
Hoil-1ΔFoxn1_C
D
Thymic cellularity (x10-7)
E
Splenic T cell %
F
TEC # (x10-4)
G
mTEC # (x10-4)
H
cTEC # (x10-3)
Hoil1lox/lox
Hoil1lox/loxCasp8-/-MLKL-/-
Hoil1ΔFoxn1
Hoil1ΔFoxn1Casp8-/-MLKL-/-
I
Hoil1lox/lox
Hoil1lox/loxCasp8-/-MLKL-/-
Hoil1ΔFoxn1
Hoil1ΔFoxn1Casp8-/-MLKL-/-
K8
K5
UEA-1
J

Figure 5

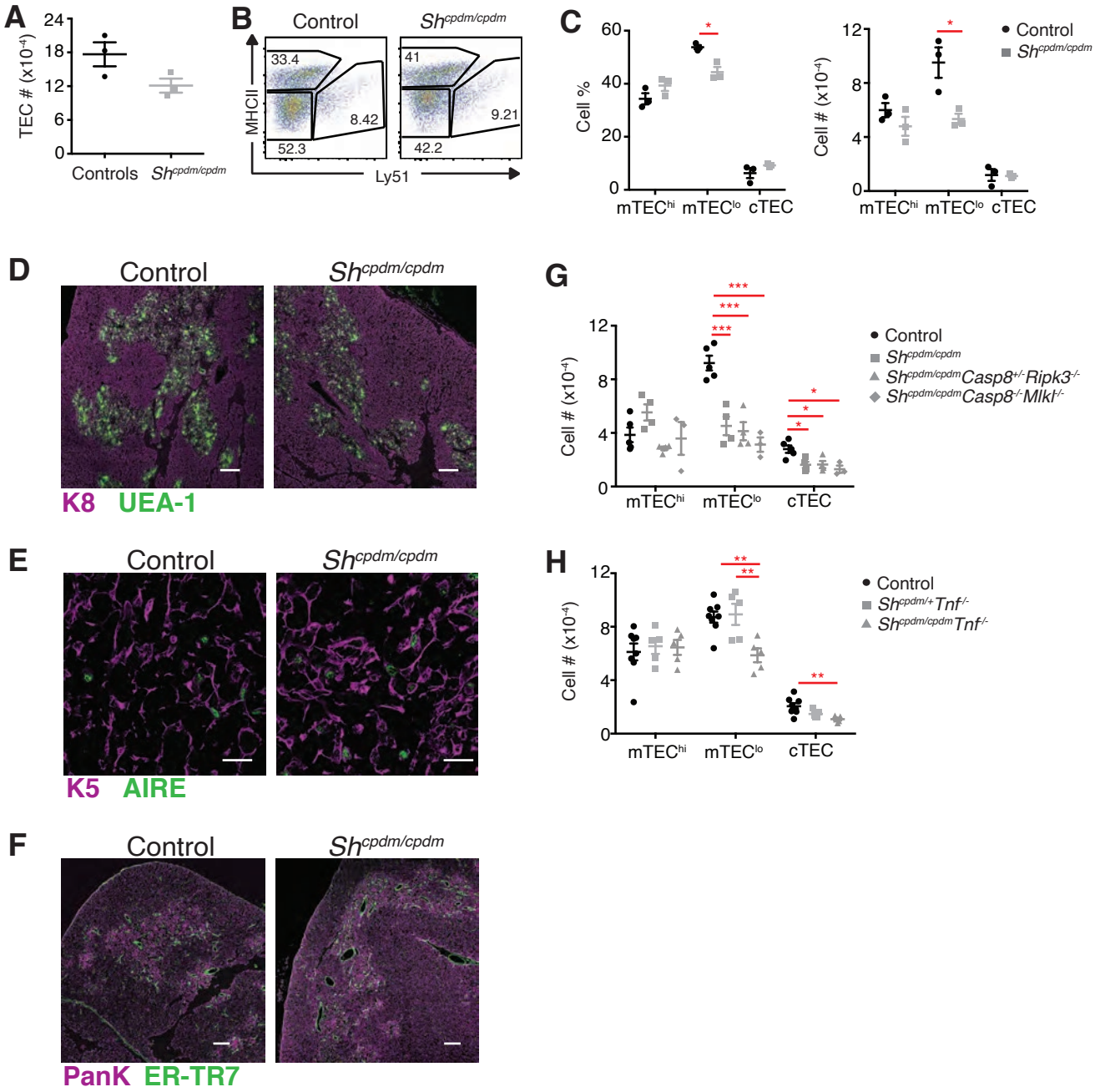
A
TEC # (x10⁻⁴)
24
18
12
6
0
Controls
Shcpdm/cpdm
B
Control
Shcpdm/cpdm
MHCII
Ly51
33.4
8.42
52.3
41
9.21
42.2
C
Cell %
60
40
20
0
mTEChi
mTEClo
cTEC
Cell # (x10⁻⁴)
12
8
4
0
Control
Shcpdm/cpdm
D
Control
Shcpdm/cpdm
K8
UEA-1
E
Control
Shcpdm/cpdm
K5
AIRE
F
Control
Shcpdm/cpdm
PanK
ER-TR7
G
Cell # (x10⁻⁴)
Control
Shcpdm/cpdm
Shcpdm/cpdmCasp8+/-Ripk3-/-
Shcpdm/cpdmCasp8-/-Mlkl-/-
H
Cell # (x10⁻⁴)
Control
Shcpdm/+Tnf-/-
Shcpdm/cpdmTnf-/-